Available online at www.sciencedirect.com

ScienceDirect

Ceramics International 40 (2014) 2237–2247

CERAMICS INTERNATIONAL

www.elsevier.com/locate/ceramint

Enhanced biocorrosion resistance of surface modified magnesium alloys using inorganic/organic composite layer for biomedical applications

Abdalla Abdal-hay[a,b,c], Montasser Dewidar[d], Juhyun Lim[e], Jae Kyoo Lim[c,*]

[a]Department of Bionano System Engineering, College of Engineering, Chonbuk National University, Jeonju 561-756, Republic of Korea
[b]Department of Engineering Materials and Mechanical Design, Faculty of Engineering, South Valley of University, 83523 Qena, Egypt
[c]Department of Mechanical Design Engineering, Chonbuk National University, Jeonju 561-756, Republic of Korea
[d]Department of Materials and Mechanical Design, Faculty of Energy Engineering, Aswan University, Aswan, Egypt
[e]Department of Urology, University of Ulsan, College of Medicine, Gangneung, Republic of Korea

Received 25 June 2013; received in revised form 13 July 2013; accepted 29 July 2013
Available online 7 August 2013

Abstract

Magnesium (Mg) is a very active element with low surface stability. Thus, the biocorrosion resistance of Mg and its alloys in electrolytic physiological environments is extremely poor, which is the main limitation preventing their use in biomedical applications. In addition, generating an appropriate protective layer to coat the surface of such materials is a challenge due to the low level of surface stability. The aim of this study was to prepare thin Ti-O films on Mg substrates using electron beam physical vapor deposition (EB-PVD) in order to improve the surface stability of Mg. To provide further corrosion resistance and facilitate improved bioactivity and biocompatibility, Ti-O thin films were subsequently coated with PLA as a top layer by dip-coating. The surface properties of the coated layers were characterized by AFM, X-RD, FTIR, SEM, and EDS. Furthermore, the biocorrosion characteristics of samples were measured by electrochemical corrosion and hydrogen evaluation tests in standard simulation body fluid (SBF) at 37.5 °C. Our results showed that incorporation of a composite layer significantly reduced the rate of degradation of Mg alloys, particularly during the initial immersion stages. The rates of hydrogen evolution of Mg bars with and without a Ti-O/PLA composite coating after 18 days was approximately 4.86 and 13.4 ml cm^{-2}, respectively. Together, these results demonstrated that surface treatment of Mg substrates with Ti-O and PLA, together with the associated changes of surface reactivity and chemistry, provide a viable strategy to facilitate cell survival on otherwise non-biocompatible Mg surfaces.

Keywords: B. Composites; Magnesium alloys; Polymers

1. Introduction

In recent years, magnesium (Mg) and Mg alloys have received a growing amount of attention in various applications such as aerospace, electronics, automotive parts, and biomedical fields. Specifically, the excellent properties of Mg alloys such as their low density, high specific strength, excellent castability, appropriate corrosion rates in physiological media, and good electromagnetic shielding make Mg alloys preferable as implant materials and appealing for use in cardiovascular interventions and osteosynthesis applications [1,2]. Biodegradability and inherent biocompatibility are preferable advantages of Mg alloys, which have been observed in both clinical and in vivo and in vitro assessments [3–5]. Due to the biodegradability of Mg based implant materials, additional surgeries to remove implants can be avoided. Importantly, the ability to avoid repeated surgeries not only decreases the morbidity rate of patients, but also results in decreased health care costs and shortened hospitalization [6].

Unfortunately, Mg and its alloys have disadvantages that limit their use to a broad range of applications, particularly in the biomedical fields. Indeed, a major concern is the very low surface stability of Mg and Mg alloys, which causes them to

*Corresponding author. Tel.: +82 63 20 2321; fax: +82 63 270 4439.
E-mail address: jklim@jbnu.ac.kr (J.K. Lim).

0272-8842/$ - see front matter © 2013 Elsevier Ltd and Techna Group S.r.l. All rights reserved.
http://dx.doi.org/10.1016/j.ceramint.2013.07.142

corrode quickly in aqueous environments [7]. In Mg and Mg alloys, elemental impurities and cathodic sites with low hydrogen overpotential facilitate hydrogen gas evolution, causing substantial galvanic corrosion and the potential to create local gas cavities *in vivo* [8]. Environment conditions, surface properties, alloy chemistry, and metal impurities are additional factors that affect the corrosion behavior of Mg. Suitable techniques to control general corrosion, such as new bioengineering alloys [9–13] or/and addition of rare-earth elements [14] do not provide improved protection against galvanic corrosion, and in fact hinder the desirable high degradation rates of Mg based implants in early stages after implantation. Furthermore, new advanced alloys may be subjected to severe localized corrosion characterized by inhomogeneous corrosion on the surface and severely corroded sites [15,16]. This type of corrosion is sufficient to deteriorate mechanical integrity before tissue has sufficient time to heal. Therefore, development of specific biocompatible coating materials that can control the rate of degradation of metallic biomaterials is necessary. Organic coatings are well known to enhance corrosion resistance and have been applied in a wide number of applications. In addition, polymeric coatings have been used not only to alter the rate of Mg degradation, but also to produce superior biocompatibility and biostability [4], thromboresistance, antimicrobial action, dielectric strength, wear properties, and lubricity [17], and may make the use of medical implants within the body both more feasible and desirable. In the present study, poly(lactic acid) (PLA) was used as a top-coating film. PLA is used primarily in surgical and biomedical applications [3,18]. PLA has interesting mechanical properties in comparison with standard polymers. Another major advantage of PLA is that it has good adhesion properties in comparison with synthetic biopolymers [19]. Numerous studies have reported that the corrosion protection afforded by specific types of coatings depends more on adhesion bonding than on the diffusion of corrosive specimens through the coating [20]. Many studies have investigated polymeric coatings Mg based alloys [21–25]. In fact, since the surface of Mg is often regarded as inherently unstable in physiological environments, direct polymeric coating on the surface of Mg may not provide sufficient adhesion, thereby allowing water molecules to diffuse easier through the coating, resulting in the protective layers becoming steeply delaminated and removed from the substrate. Zheng et al. coated Mg with multiple layers of chitosan, but reported that the coatings did not provide promising protection [21]. In general, organic coatings result in poor adhesion if applied without appropriate pre-treatment [26]. Thus, numerous methods of chemical modifications have been applied to improve the stability and adhesion between organic layers and Mg substrates [23,27–32]. However, a chemical treatment capable of generating a desirable improvement in degradation performance in physiological environments has not been identified. Therefore, the development of specific coating biomaterials devoted to improve the surface stability of Mg remains a significant challenge. To address this problem, fabricating compact titanium oxide (Ti-O) films below organic coatings appears to have excellent potential to achieve both corrosion protection and surface stability without adversely affecting mechanical properties. Indeed, uniform Ti-O layers on 316L and Ni–Ti stents exhibit superior blood biocompatibility compared with low-temperature isotopic pyrolytic carbon [33,34]. Furthermore, films of nano-size thickness and good biocompatibility may be acceptable for use in the human body compared with permanent substrates.

The aim of this present study was to fabricate Ti-O thin films prior to coating with PLA in order to improve the surface stability of Mg alloys, thereby modifying both the adhesion properties and overall biocorrosion resistance of Mg alloys under physiological conditions. In addition, we investigated the degradation performance of Ti-O/PLA composite surface coatings in SBF as a function of immersion length by measuring both hydrogen gas evolution and changes in pH.

2. Experimental work

2.1. Substrate pre-deposition

Die casting Mg alloy AM50 was chosen as a substrate to validate degradation rates and corrosion behavior under test conditions. The chemical composition of AM50 alloy is listed in Table 1. AM50 was cut into square specimens with dimensions of $12 \times 12 \times 2\ mm^3$ (total surface area: $3.83 \pm 0.2\ cm^2$). Prior to e-Beam coating, samples were mechanically polished with silicon carbide paper (grit range 400–2000) followed by polishing with 1 μm diamond grinding to mirror the surface. Samples were then cleaned ultrasonically in acetone for 5 min to remove residual grease and then transferred to distilled water. The treated specimens were then dried for the deposition procedure.

2.2. Coating procedures

Ti-O coating layers were formed on treated samples by electron beam physical vapor deposition (EB-PVD). An e-beam evaporator system (KVE-C25096) was employed for experiments. The deposition target material used in the experiment was commercially pure titanium (c.p. Ti) with high purity of 99.995% (c.p.Ti was supplied by TASCO, USA, in the form of $6 \times 6\ mm^2$ pellets). To avoid becoming

Table 1
Chemical composition of the substrate in weight percentage (wt%).

Element	Al	Mn	Zn	Si	Ni	Cu	Fe	Be	Mg
(wt%)	4.9	0.45	0.2	0.047	0.00095	0.008	0.004	0.001	Bal

contaminated by the evaporant, the gun assembly was located outside the evaporation zone. After the chamber was evacuated to 5.0×10^{-3} Torr, a high vacuum of 2.0×10^{-7} Torr was attained using a cryo pump. The substrates were then cleaned by sputtering using an argon ion beam for 15 min. Next, an e-beam was generated at a voltage of 9 kV to heat the evaporant. A vapor flux was generated for Ti-O deposition on the rotating substrate at a rate of 6.0 rev min^{-1} in order to improve uniformity of the coating layer. The total layer thickness was controlled as a function of time and feed rate according to the following parameters: 0–10 min, 0.5 Å/s; 10–30 min, 1.5 Å/s and 30–38 min, 0.2 Å/s. Film thickness was monitored by a quartz balance installed inside the evaporation chamber adjusted to an accuracy of ± 10 nm. A tungsten heater was used prior to and during the deposition procedure to heat the substrates to an average temperature of 120 °C.

PLA was used as a top-coating layer and was purchased from Dow Cargill (Minneapolis, MN). The weight-average and number-average molecular weights of PLA were 148,000 and 110,000 Da, respectively. Dichloromethane (DCM) was used as solvent and supplied from SHAWA, Japan without further purification. PLA was prepared as a 4 wt% concentration by dissolving the polymer in DCM at room temperature and stirring gently to form a transparent solution. The prepared Mg alloy substrates coated with Ti-O films were then immersed into the polymer solution for 30 s to allow wetting. In order to obtain a stain-free surface, the specimens were slowly pulled out of the solution at an approximate rate of 2 mm/s. Prior to dip-coating, all of the specimens were placed on a hot plate at 160 °C for 10 min to remove moisture and entrapped air from the substrate surface. Finally, the coated samples were introduced to a vacuum oven (10 mbar) for 12 h at a temperature of 50 °C.

2.3. Characterization

The thickness of deposited layers on the coated samples was measured using an Alpha step instrument (KLA-TENCOR Alpha Step IQ). Thickness estimation was performed as described previously [3]. The surface morphology and root mean square (RMS) surface roughness values of titanium oxide deposited layers were characterized by atomic force microscopy (AFM, MultiMode/BioScope, CJ10). Topographic and phase images were recorded simultaneously with a standard silicon tip on a cantilever beam.

The structure of titanium films was investigated by X-ray diffraction (X-RD, Rigaku) with parallel beam geometry using Cu-$K_{\alpha 1}$ radiation. Due to the reflectometry of the diffractometer, samples were aligned exactly at the goniometer center. The effective penetration depth of the X-ray beam was approximately 420 nm. Fourier transform infrared spectrometry (FT-IR) analysis was used to determine the purity of PLA in the top coating layer. FT-IR spectra in transmission mode were collected using an ABB Bomen MB100 spectrometer (Bomen, Canada) with an FT-IR 5000 in the range of 4250–400 cm^{-1}.

Surface properties of the composite coatings were characterized using a JEOL JSM 820 scanning electron microscope (SEM) coupled with energy dispersive spectrometer (EDS). Due to the lack of surface conductivity, PLA-coated samples were sputtered with platinum prior to SEM observation.

Adhesion testing was used to investigate the mechanism of adhesive Ti-O/PLA composite films on Mg substrate. Pull-off adhesion testing of the coating was performed according to the procedure described in ASTM D 4541. Adhesion testing of coated samples was carried out in both wet and dry conditions. For the wet adhesion test, treated samples were immersed for 12 h at 37 ± 0.2 °C in simulated body fluid (SBF), which has an ionic composition and concentration similar to that of human plasma. Before soaking samples, a dolly 20 mm in size was adhered to the coating surface using Araldite Epoxy adhesive and cured at room temperature for 24 h. After immersion, a pull-off test was conducted using an Elcometer adhesion tester (England). Three to four measurements were performed for each sample.

The electrochemical behaviors of both uncoated and coated samples were investigated by potentiodynamic polarization test (263A, EG&G PAR, USA) conducted in standard simulated body fluids (SBF) at pH 7.4. A three-electrode cell was used, consisting of the sample as the working electrode, Ag/AgCl/1 M KCl (Satd.) as the reference electrode, and platinum as the counter electrode. The area of the working electrode (controller and deposited layer samples) that was exposed to the solution was 0.785 cm^2. A 1 mVs^{-1} scanning rate was applied during the potentiodynamic polarization test. The changes in free corrosion potential (E_{corr}) were monitored as a function of time. Temperature was controlled at 37 ± 0.5 °C during the test. The results of the corrosion test of the samples were calculated by extrapolating the polarization curve according to ASTM-G102-89. Prior to electrochemical corrosion testing, the samples were immersed in 1000 ml of SBF for 15 min to establish a relatively stable open circuit potential [4].

Immersion tests were performed in SBF (Hank's balanced salts, H2387, Sigma Aldrich, Korea). Three specimens for each condition were immersed in 100 ml of solution (the ratio of surface area to solution volume was 1:35 cm^2/ml) such that they were not touching each other or the container wall. The temperature was controlled at 37.5 ± 0.2 °C during the test by using a water flow bath. The electrolyte was saturated with atmospheric oxygen and was not stirred during experiments. Immersed samples were removed at 1, 3, 7, 8, 10, 12, 15, and 18 days. At the time of removal, samples were gently rinsed with flowing distilled water and dried at room temperature to avoid cracking. After immersion, surface morphology was examined by scanning electron microscopy (SEM). The degradation rate was determined by measuring the rate of hydrogen evolution from samples as described previously [35]. For optical microscope observation (LEICA Microsystems EZ4D), the coated and uncoated samples were immersed in a chromic acid solution (200 g/L Cr_2O_3+10 g/L $AgNO_3$) for 10 min to remove residual polymer and corrosion products. The samples were then soaked in distilled water and acetone for a few seconds, followed by drying with warm flowing air

(40 °C). Hydrogen evolution and pH (Hanna Hi 8314 pH meter, Romania, Europe) were measured as a function of time.

Analysis of cell attachment was performed as described previously by our group [36,37]. Briefly, MC3T3 osteoblast cells were cultured in Dulbecco's modified Eagle's medium (DMEM) (Gibco Co, USA), supplemented with 10% fetal bovine serum (FBS) in a humidified incubator with 5% CO_2 and 95% relative humidity at 37 °C. The protocol for culturing cells with coated and uncoated samples was established using a direct contact method. Prior to cell culture, the samples were sterilized by ethylene oxide (EO) gas. Cells were incubated in 24-well flat-bottomed cell culture plates at 5×10^4 cells/ml medium in each well and incubated for one day to allow cell attachment on the surface of the samples. After that, culture media was replaced with 1 ml of extraction medium. After incubation in a humid atmosphere for 24 h, cells were fixed in PBS containing with 3% formaldehyde and 0.2% glutaraldehyde and stained with 0.3% crystal violet. Cell morphology was observed by low voltage Bio-SEM (HITACHI, S-3000N) at an acceleration voltage of 10 kV.

3. Results and discussion

EB-PVD is a popular technique in thin film deposition to produce various coatings [38]. Specifically, the use of EB-PVD may facilitate improvement of several advantageous properties such as purity, homogeneity, uniformity, and density of coatings, as well as providing for variable thickness and simplicity of preparation. For these reasons, EB-PVD was used for preparation of Ti-O thin film on Mg bar substrates. The Surface morphology of a typical thin film coated Mg substrate, which was successfully fabricated by EB-PVD, is shown in Fig. 1; a 1.5 μm × 1.5 μm area was evaluated. The thin film deposited on substrates exhibited a flat and porous surface morphology, as well as grain features. However, a strong coalescence of neighboring grains was observed, as shown in Fig. 1A. The RMS surface roughness measured over the given area was approximately 6.3 nm, which is relatively high compared with values reported in the literature [39]. The relatively uniform and porous surface morphology, as depicted in Fig. 1B, may have been due to changes in the rate of evaporation during the entire coating period as mentioned in the experimental section. These results were in agreement with those of a previous study [39]. The roughened surface or/and presence of small voids and enlargements on the surface allowed the polymer solution to penetrate into crevices and pores, which upon coating, became mechanically embedded in the metal surface and surface oxide structure. The cavities and pores formed during Mg surface treatment provided a larger surface area for electrochemical interaction, which further increased the adhesive strength of the polymer coating layer.

X-ray and EDS patterns of Ti-O thin films deposited on Mg bar are shown in Fig. 2. Mg peaks were clearly observed by XRD, whereas no diffraction peaks attributed to crystallized titanium dioxide were observed (as shown in Fig. 2A.). This observation was attributed primarily to the thickness of the titanium film, which was smaller than 100 nm and did not yield sufficient XRD signals to identify TiO_2 peaks, and may have also been influenced by the Ti-O film exhibiting amorphous behavior [40]. Elements of the corresponding EDS spectrum deposited on the substrates were clearly identified in the titanium deposited film, and consisted primarily of three elements: Mg, O, and Ti (Fig. 2B). Compared with the elemental composition of the EDS spectrum, the Ti signal exhibited a very low intensity compared with Mg, which was related to their respective thicknesses in the deposited film.

It is important to note that the biological performance of implants depends significantly on the initial interactions that take place when the implant surfaces come into contact with the biological environment. For this reason, PLA was selected

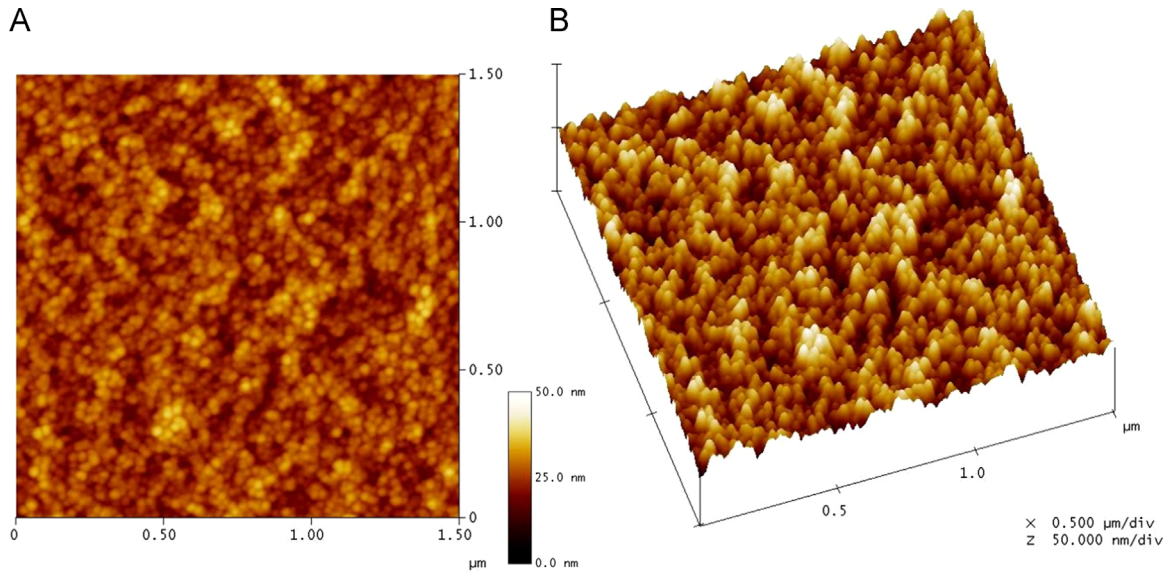

Fig. 1. AFM images of Ti-O thin film (thickness ~ 100 nm) coated Mg alloy generated by EB-PVD: (A) 2-D image and (B) 3-D image.

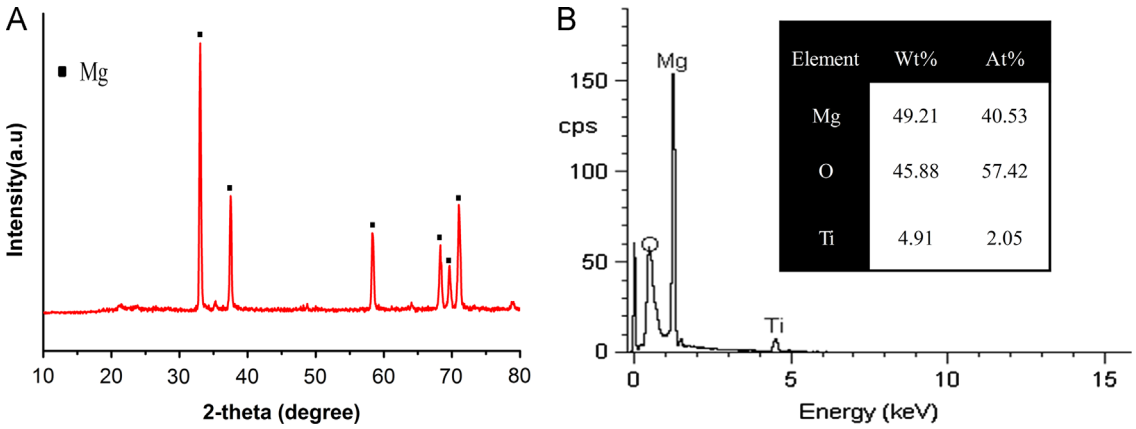

Fig. 2. Surface analysis of Ti-O thin film coated Mg bars by (A) XRD and (B) EDS.

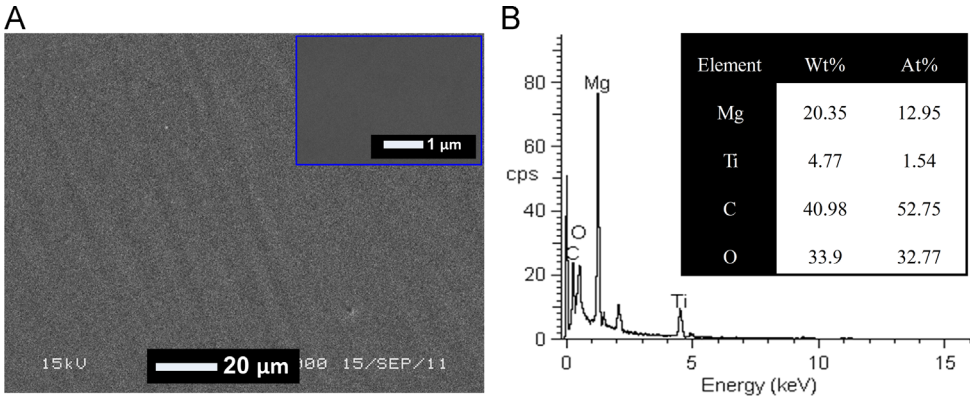

Fig. 3. (A) SEM surface analysis and (B) EDS element concentrations for Ti-O/PLA composite coated Mg alloy. (Inset, A) Higher magnification analysis.

as the top-coating layer, as it is an FDA-approved biodegradable polymer. Furthermore, the degradation products of PLA are non-acidic and have been shown to induce deposition of calcium-phosphate compounds in vivo [41]. In the present study, the PLA-deposited layer on Mg bar was prepared by dip-coating technique with a 4 wt% solution. FTIR analysis was used to verify the chemical structure of PLA, and FTIR spectra are shown as supplementary data (see Fig. S1). Transmittance bands at approximately 1453, 1750, and 2826–2995 cm^{-1} in all spectra were attributed to the vibrations of –C–H stretch, –C=O stretch, and C–H bend in PLA, respectively. Representative SEM photographs of Ti-O/PLA composite coating samples are shown in Fig. 3A. If an anticorrosive coating has a defect, which is often the case in practice, and is exposed to the elements, corrosion may be initiated much more rapidly compared with a defect free surface. In the present study, the morphology of the top surface of the composite coating (organic layer) exhibited a smooth and flat surface, was free of voids and porosity, and surprisingly, had a dense transparent top layer. Specifically, there was an unexpected formation of a non-porous phase structure on the surface structure formed by PLA as we had anticipated that the PLA/DCM solution would generate a porous phase structure at the concentrations used in the study. Based on our results, PLA/DCM (10/90) (viscosity 285.5 cP) generates a network with porous morphology and an average pore size of 2.86 µm [42]. However, for the 4 wt% polymer solution deposited layer, the solution viscosity and layer thickness were 13.2 cP and 1.8 ± 0.23 µm, respectively.

We hypothesized several possible mechanisms to explain the formation of the non-porous structures. First, when the samples were removed from the solution, gravity simultaneously forced the solution downwards. Thus, it may have been possible that the speed of the outflow increased with decreasing viscosity, i.e. a lower viscosity led to a lower drag acting in the opposite direction of the gravity force, resulting in higher solution outflow and decreased thickness. Thus, the solution outflow from top to bottom on the former deposited layer may have closed the porous formation. Another possibility is that due to its low thickness, the solution may have been unable to provide a polymer-poor phase. A polymer coating contains three films, namely, the primer, intermediate, and top film, the properties and functions of which have been described previously [42]. Furthermore, the high temperature of the drying step (50 °C) may have induced a phase inversion process governed by solvent evaporation, which could have resulted in a dense morphology. Accordingly, a decorative film (top-film) in the porous phase structure could not have been established due to the low thickness. It has been proposed that decreasing the thickness of organic coatings may lead to good mechanical stability of the polymer as it becomes more and more flexible and also gains adhesion to the metal surface [43].

The advantages of lightweight properties of Mg alloy may be lost if the thickness of the applied coating is increased. However, we found that altering the thickness of PLA films can be used successfully to address this dilemma. Specifically, the dense phase structure was favorable for providing corrosion protection during the early stages of implantation as well as degradation in future applications due to decreased contact area with the surrounding solution. These observations confirmed that surface phase structures depended not only on the solvent evaporation rate, but also the specific solvent–polymer system. However, further investigations into PLA/DCM systems are required to confirm and extend our results.

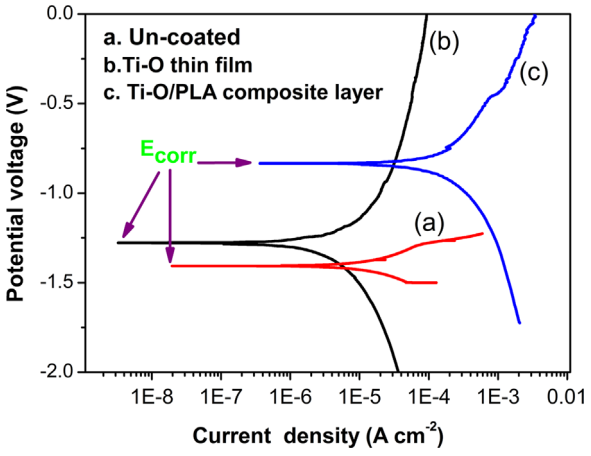

Fig. 4. Potentiodynamic polarization curves of uncoated and coated samples showing positive corrosion behavior for treated samples.

As shown in Fig. 3B, EDS clearly identified only the elements of Mg, titanium, carbon and oxygen, indicating that the Ti-O/PLA composite coating Mg alloys were free of any impurities. The carbon signal was attributed to the PLA-deposited layer.

Most organic coatings adhere to metals by hydrogen bonding or forming secondary bonds, which include dispersion forces, dipole interactions, and van der Waals forces. According to a previous study [42], that investigated the adhesion mechanism and adhesion performance of PLA layers on Mg substrates, PLA-coated Mg exhibits good adhesion strength in dry conditions. However, the strength of PLA-coated Mg decreases dramatically after immersion for 12 h in SBF, mainly due to the instability of the Mg surface upon exposure to physiological conditions. In the present study, the adhesion strength of Ti-O/PLA composite coatings exhibited almost identical adhesion strength compared with dry condition (6.12 ± 0.54 MPa). Further, Ti-O/PLA significantly improved adhesion strength after immersion in SBF for 12 h (4.32 ± 0.23 MPa). Therefore, the Ti-O thin film improved the stability of Mg substrates as well as adhesion strength, which was attributed to Ti-O inhibiting formation of a direct interface between water molecules and the Mg substrate at the initial stages of exposure.

Corrosion reactions at metal/polymer coating interfaces are electrochemical in nature. As such, electrochemical techniques are used in evaluating the protective performance of inorganic–organic coating. Representative potentiodynamic polarization curves obtained from uncoated and coated AM50 Mg samples (Ti-O and Ti-O/PLA) in SBF at 37 °C are shown in Fig. 4.

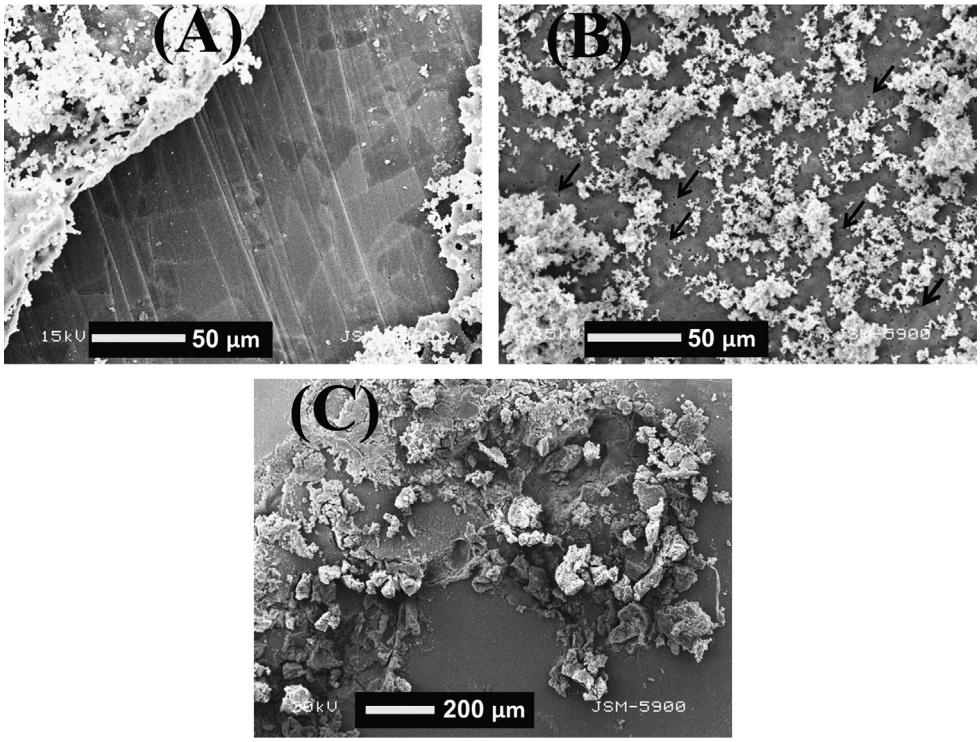

Fig. 5. Selected images for surface morphology in SEM after immersion in SBF for 15 days: (A) PLA-layer, (B) Ti-O/PLA composite layer and (C) uncoated samples. Arrows in Fig. 5B show the formation of pinholes on the composite layer.

Compared to the corrosion potential (E_{corr}) of uncoated AM50 substrate (−1405 mV), the E_{corr} of the Ti-O/PLA composite coated Mg substrate (−834 mV) shifted in a positive direction, and were 40% higher than uncoated samples. Conversely, the corrosion potential (E_{corr}) of titanium oxide thin films deposited on the Mg substrate was −1280 mV. Specifically, Mg substrates coated with composite films seemed to have a higher anticorrosion performance than AM50 alloy with a Ti-O film coating alone, indicating that the PLA dense layer closed and covered the pores present on Ti-O film-deposited Mg. The interaction between the electrolyte solution and Mg substrate during the first immersion period was prevented. Thus, Mg based alloys coated with Ti-O/PLA may be a promising candidate to enhance the corrosion resistance of Mg.

Fig. 5 shows SEM profiles of surface degradation of PLA and Ti-O/PLA composite layer coated samples, as well as a bare Mg bar, after immersion in SBF for 15 days. As corrosion resistant coating should significantly delay initiation of biodegradation, it should be noted that Mg substrate degradation occurred at areas where the coating was damaged. As observed in Fig. 5A, the samples coated with PLA alone exhibited the worst layer defects and delamination compared with a Ti-O/PLA coating after exposure to the SBF solution. However, in both cases, it was clear that that the Mg surface was not deteriorated, as shown by analysis of the peeling area (Fig. 5A). During exposure to the SBF solution, some bubbles emerged from the surface, indicating that gas formation may have penetrated the intermediate polymer layer [42]. Delamination damage results from bonds breaking at the polymer–metal interface, resulting in alkalinity of cathodic reaction products [44,45]. Subsequently, evolution of gas resulted from the galvanic cell with anodic and cathodic regions [46].

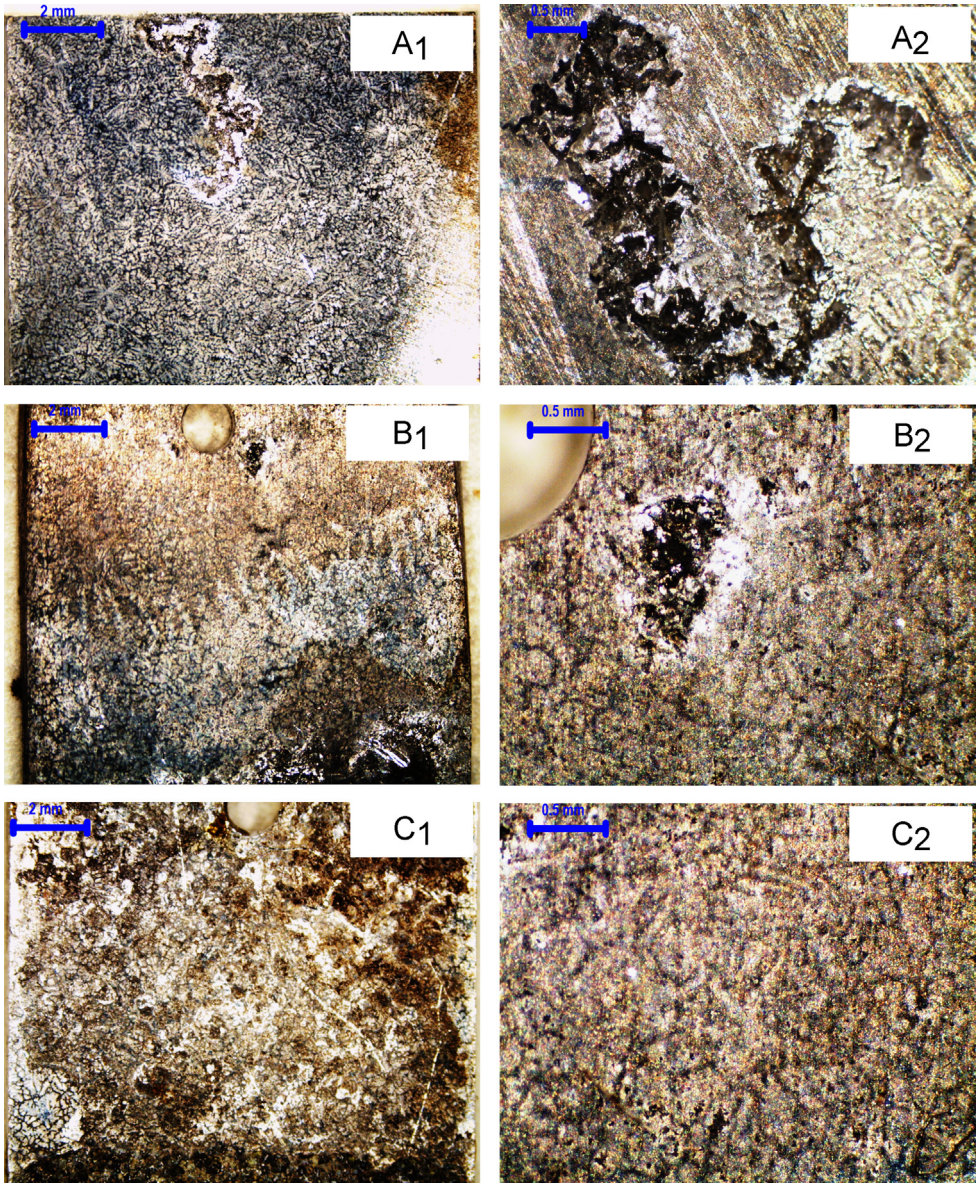

Fig. 6. Typical surface appearance by optical microscopy immersed in SBF for 20 days after removing corrosion products for (a) uncoated samples, (b) samples coated with PLA, and (c) samples coated with a Ti-O/PLA composite layer. Numbers 1 and 2 indicate low and high magnifications, respectively.

In contrast, samples coated with a composite layer lasted without defects, and uniform pinholes (arrows shown in Fig. 5B) were generated on the polymer-coated layer. These pinholes were formed mainly due to Mg corrosion, and indicated that the presence of the thin Ti-O film improved both the stability of the Mg surface as well as corrosion potential without totally invalidating the degradation of Mg substrates in SBF due to micro pores present on the film. Consequently, hydrogen gas evolution could have easily been relieved through the coating layers (i.e. osmotic pressure and back diffusion of molecules were approximately equal). The electrochemical reaction (1) describing this phenomenon is shown below

$$Mg_{(s)}+2H_2O \rightarrow Mg^{2+}+2OH^{-}_{(aq)}+H^{\uparrow}_{2(g)}(\text{overall reaction}) \quad (1)$$

The composite coating did not show blistering and/or peeling during the early stages of immersion. We speculated that the composite coating minimized Mg ion release simultaneously with hydrogen gas evolution, which could then be uniformly relieved through regularly formed pinholes. Indeed, numerous studies have reported that low rates of degradation decrease the evolution of hydrogen gas around the host tissue at early stages during implantation. However, Witt et al. [14] found that hydrogen gas bubbles appear within one week after implantation, but vanish after 2–3 weeks. In the present study, the rate of corrosion decreased with increasing length of immersion due to the formation of corrosion products. However, the composite coating was sufficient enough to dampen the evolution of hydrogen gas at an early stage. Importantly, a promising degradation rate (i.e. low release of Mg ions) may result in a rate of hydrogen gas release similar to rates of absorption and diffusion into the surrounding tissues [47], thereby avoiding undesirable hydrogen gas evolution [42]. On the other hand, unprotected samples exhibited significant surface breakdown and unfavorable rates of degradation as illustrated in Fig. 5C.

Fig. 6 depicts the surface appearance of samples immersed in SBF for 18 days as determined by optical microscopy. Corrosion products were removed to more closely study the biocorrosion behavior of Mg bar and coated samples. We observed that the surface of the untreated samples showed inhomogeneous corrosion and severely corroded sites, which appeared to initiate from samples edges. This observation indicated that vulnerable surfaces were under severe localized corrosion, which caused a significant granular attack as observed after the surfaces were cleaned (Fig. 6A_1 and A_2). The Mg substrates coated with PLA exhibited only limited evidence of localized corrosion as shown in Fig. 6B_1 and B_2. Specifically, small defects like scratches or tiny pores in micro or nano-scales, which allowed the electrolyte to reach the metallic substrate, may have triggered localized corrosion. In contrast, as shown in Fig. 6C_1 and C_2, samples coated with a composite layer did not exhibit any deterioration, whereas micro pitting corrosion was observed on the cleaned surface. Thus, the presence of the composite coating will likely help delay hydrogen evolution and subsequently decrease the rate of degradation of Mg during the early healing period after implantation.

Environmental properties such as pH are the governing conditions that determine the performance of composite coatings. Fig. 7A shows a graph of pH measurements for the composite coating and Mg alloy coupons as a function of immersion time in SBF. During corrosion of Mg in the initial immersion stages, a large amount of Mg ions dissolved into the test solution and the pH increased according to reaction (1). Specifically, a pH value of 8.5 was recorded after 12 h for uncoated samples, which was taken as an indication of the formation of Mg hydroxide. Conversely, samples coated with the composite layer were unchanged after four days. Thus, our results confirm that water molecule did not penetrate the composite layer to react with the sample substrate. The change in pH value was believed to play a crucial role in the corrosion behavior of Mg based alloys.

Rates of hydrogen gas evolution of immersed samples are given in Fig. 7B. As discussed above, the hydrogen evolution rate is related to the dissolution of Mg. According to hydrogen evaluation test, a steep rise in the release of hydrogen gas for unprotected samples in the immersion bath was observed during the first 12 h (0.5 day), which was recorded as

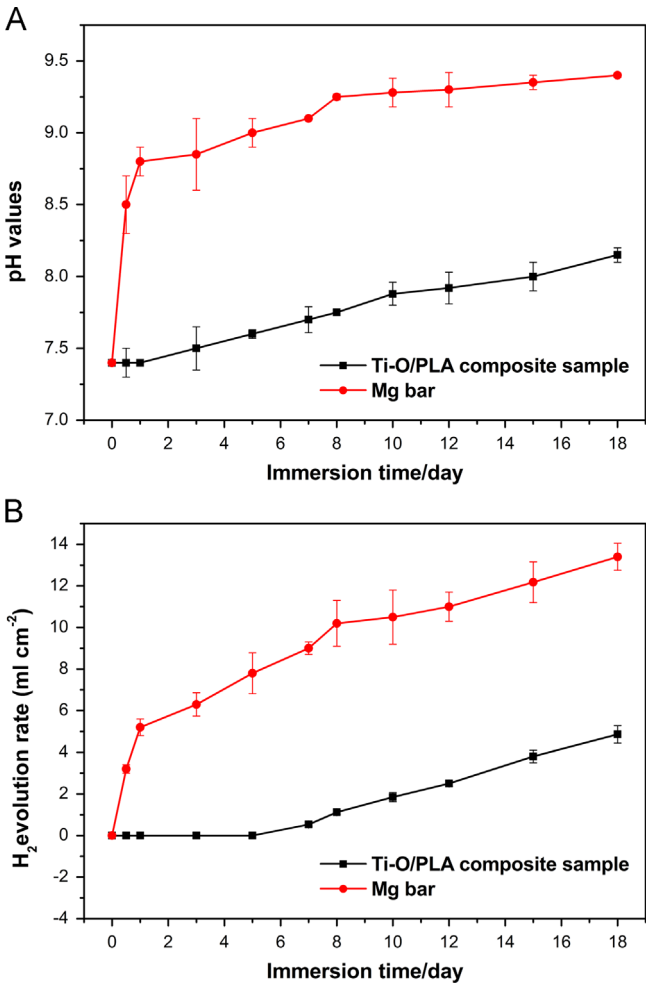

Fig. 7. (A) pH measurements and (B) hydrogen evolution rates as a function of immersion time.

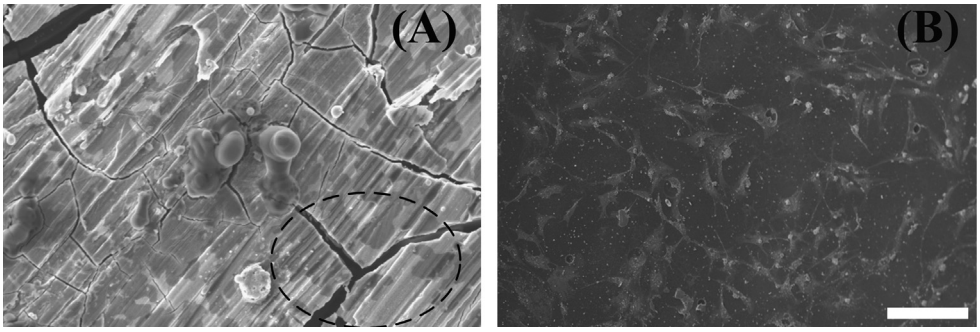

Fig. 8. MC3T3 osteoblast cells were cultured by the direct contact method on uncoated (A) and (B) composite coated samples. The marked area in A shows localized corrosion of the uncoated sample.

approximately 3.2 ml/cm^2. On the other hand, Ti-O/PLA composite-coated samples hardly formed any hydrogen in the early stages of exposure to SBF. A longer immersion time resulted in a decreased rate of hydrogen release from unprotected samples, with a recorded value of 13.4 ml/cm^2. This result indicated that the precipitation of corrosion products either decreased the rate of corrosion [48] or, more likely, the equilibrium between the formation and dissolution of established corrosion products, leading to stable degradation rates. However, based on the accumulation of these products, H_2 was still very high in comparison with treated samples, which were significantly lower (4.8 ml/cm^2) after immersion for 18 days. The rates of hydrogen evolution were in agreement with pH measurements, and it was obvious from our experiments that the composite coating dramatically improved corrosion resistance of Mg alloy after immersion in simulation body fluid (SBF), particularly during the initial stages. Together, these results indicated that the composite coating successfully delayed biodegradation of the substrate.

In vitro cytocompatibility evaluation is a basic biological assay performed for biomaterials, and can be very helpful in determining interactions between cells and biomaterials interaction. In the present study, cell attachment and survival were analyzed using two types of samples, namely, uncoated substrate and substrate coated with an inorganic–organic composite layer. The results of cell attachment and survival after culture for 1 day are shown in Fig. 8. The biocompatibility of modified samples was evaluated by observing the attachment of seeded MC3T3 osteoblasts. A remarkable number of cells were found to be attached on Ti-O/PLA composite layer modified Mg, whereas no cells were attached on pristine Mg (Fig. 8A and B). For the uncoated sample, only a very few, less round cells were observed, whereas the coated sample exhibited a much larger number of cells that were flat in shape and spreading. Together, these results indicated that uncoated Mg does not promote cell survive and attachment. This result is in contrast with numerous reports indicating that Mg is a biocompatible implant material. Specifically, Lorenz et al. [49] found that a large range of factors including H_2 gas evolution, increased pH due to Mg dissolution in cell culture medium, as well as chemical and physical properties of native or corroded Mg surfaces may contribute to decreased cell adhesion and survival on pure Mg substrates compared with modified Mg substrates.

Theoretical calculations indicate that in a neutral solution, the pH directly at the surface of Mg is always greater than 10. With a fast hydrogen evolution process, local alkalization is inevitable around a rapidly corroding Mg implant. Thus, local alkalization can unfavorably affect the balance of pH dependent physiological reactions in the vicinity of a Mg implant, and may even lead to an alkaline poisoning effect if the local in vivo pH value exceeds 7.8 [10]. Indeed, these factors were attributed to the lack of attachment and survival of cells on pristine Mg alloys. Accordingly, we developed a strategy mitigate these concerns by slowing the biodegradation (i.e. corrosion) of Mg alloys, such that Mg^{2+} ions, H_2 gas, and OH^- ions would be generated more slowly, thereby allowing the human body to gradually adjust or otherwise address biodegradation products.

4. Conclusion

In the present study, Ti-O thin films on Mg alloy substrates were successfully fabricated by EB-PVD followed by coating with a PLA polymer-coated layer, which was carried out by a dip-coating process for further protection and biocompatibility enhancement. It has been shown that Ti-O/PLA organic coatings are sufficiently permeable by water and oxygen, while typical organic coatings cannot inhibit delamination and/or blistering of polymer layers. However, the use of a composite coating layer decreased rates of corrosion and subsequent evolution of hydrogen gas. Thus, the method described here may be useful for Mg based implants during the initial stages of healing, as it would limit the formation of hydrogen gas around the host tissue. Collectively, it is important to take into account that both Ti-O thin films and final organic top coating are critical for achieving adequate corrosion protection and producing Mg based implant materials with good biocompatibility.

Acknowledgments

This study was financially supported by the Ministry of Education, Science Technology (MEST) and National Research Foundation of Korea (NRF) through the Human Resource Training Project for Regional Innovation.

Appendix A. Supporting information

Supplementary data associated with this article can be found in the online version at http://dx.doi.org/10.1016/j.ceramint.2013.07.142.

References

[1] D. Gastaldi, V. Sassi, L. Petrini, M. Vedani, S. Trasatti, F. Migliavacca, Continuum damage model for bioresorbable magnesium alloy devices—Application to coronary stents, Journal of the Mechanical Behavior of Biomedical Materials 4 (3) (2011) 352–365.

[2] Y. Zhang, G. Zhang, M. Wei, Controlling the biodegradation rate of magnesium using biomimetic apatite coating, Journal of Biomedical Materials Research Part B: Applied Biomaterials 89 (2) (2009) 408–414.

[3] A. Abdal-hay, N.A. Barakat, J.K. Lim, Hydroxyapatite-doped poly (lactic acid) porous film coating for enhanced bioactivity and corrosion behavior of AZ31 Mg alloy for orthopedic applications, Ceramics International 39 (1) (2013) 183–195.

[4] H.M. Wong, K.W. Yeung, K.O. Lam, V. Tam, P.K. Chu, K.D. Luk, K. M. Cheung, A biodegradable polymer-based coating to control the performance of magnesium alloy orthopaedic implants, Biomaterials 31 (8) (2010) 2084–2096.

[5] B. Denkena, F. Witte, C. Podolsky, A. Lucas, Degradable implants made of magnesium alloys, in: Proceedings of the 5th Euspen International Conference, Montpellier, France, 2005.

[6] M.P. Staiger, A.M. Pietak, J. Huadmai, G. Dias, Magnesium and its alloys as orthopedic biomaterials: a review, Biomaterials 27 (9) (2006) 1728–1734.

[7] G.L. Song, A. Atrens, Corrosion mechanisms of magnesium alloys, Advanced Engineering Materials 1 (1) (1999) 11–33.

[8] F. Witte, N. Hort, C. Vogt, S. Cohen, K.U. Kainer, R. Willumeit, F. Feyerabend, Degradable biomaterials based on magnesium corrosion, Current Opinion in Solid State & Materials Science 12 (5–6) (2008) 63–72.

[9] L. Xu, G. Yu, E. Zhang, F. Pan, K. Yang, In vivo corrosion behavior of Mg–Mn-Zn alloy for bone implant application, Journal of Biomedical Materials Research Part A 83 (3) (2007) 703–711.

[10] G. Song, Control of biodegradation of biocompatable magnesium alloys, Corrosion Science 49 (4) (2007) 1696–1701.

[11] D.-S. Yin, E.-L. Zhang, S.-Y. Zeng, Effect of Zn on mechanical property and corrosion property of extruded Mg–Zn–Mn alloy, Transactions of Nonferrous Metals Society of China 18 (4) (2008) 763–768.

[12] E. Zhang, D. Yin, L. Xu, L. Yang, K. Yang, Microstructure, mechanical and corrosion properties and biocompatibility of Mg–Zn–Mn alloys for biomedical application, Materials Science and Engineering: C 29 (3) (2009) 987–993.

[13] B. Zberg, P.J. Uggowitzer, J.F. Loffler, MgZnCa glasses without clinically observable hydrogen evolution for biodegradable implants, Nature Materials 8 (11) (2009) 887–891.

[14] F. Witte, V. Kaese, H. Haferkamp, E. Switzer, A. Meyer-Lindenberg, C. J. Wirth, H. Windhagen, In vivo corrosion of four magnesium alloys and the associated bone response, Biomaterials 26 (17) (2005) 3557–3563.

[15] H.S. Kim, K. Kim, H.J. Jin, I.-J. Chin, Morphological characterization of electrospun nano-fibrous membranes of biodegradable poly(L-lactide) and poly (lactide-co-glycolide), Macromolecular Symposia 224 (1) (2005) 145–154.

[16] M. Bobby Kannan, R.K. Singh Raman, F. Witte, C. Blawert, W. Dietzel, Influence of circumferential notch and fatigue crack on the mechanical integrity of biodegradable magnesium-based alloy in simulated body fluid, Journal of Biomedical Materials Research Part B: Applied Biomaterials 96B (2) (2011) 303–309.

[17] J.E. Gray, B. Luan, Protective coatings on magnesium and its alloys—a critical review, Journal of Alloys and Compounds 336 (1–2) (2002) 88–113.

[18] C.M. Agrawal, K.A. Athanasiou, Technique to control pH in vicinity of biodegrading PLA–PGA implants, Journal of Biomedical Materials Research 38 (2) (1997) 105–114.

[19] L. Xu, A. Yamamoto, Characteristics and cytocompatibility of biodegradable polymer film on magnesium by spin coating, Colloids and Surfaces B: Biointerfaces 93 (2012) 67–74.

[20] G. Grundmeier, W. Schmidt, M. Stratmann, Corrosion protection by organic coatings: electrochemical mechanism and novel methods of investigation, Electrochimica Acta 45 (15–16) (2000) 2515–2533.

[21] X.N. Gu, Y.F. Zheng, Q.X. Lan, Y. Cheng, Z.X. Zhang, T.F. Xi, D. Y. Zhang, Surface modification of an Mg–1Ca alloy to slow down its biocorrosion by chitosan, Biomedical Materials 4 (4) (2009) 044109.

[22] J.N. Li, P. Cao, X.N. Zhang, S.X. Zhang, Y.H. He, In vitro degradation and cell attachment of a PLGA coated biodegradable Mg–6Zn based alloy, Journal of Materials Science 45 (22) (2010) 6038–6045.

[23] T.F. Conceicao, N. Scharnagl, C. Blawert, W. Dietzel, K.U. Kainer, Corrosion protection of magnesium alloy AZ31 sheets by spin coating process with poly(ether imide) [PEI], Corrosion Science 52 (6) (2010) 2066–2079.

[24] K. Bai, Y. Zhang, Z. Fu, C. Zhang, X. Cui, E. Meng, S. Guan, J. Hu, Fabrication of chitosan/magnesium phosphate composite coating and the in vitro degradation properties of coated magnesium alloy, Materials Letters 73 (0) (2012) 59–61.

[25] L. Xu, A. Yamamoto, Characteristics and cytocompatibility of biodegradable polymer film on magnesium by spin coating, Colloids Surf B Biointerfaces 93 (2012) 67–74.

[26] R.-G. Hu, S. Zhang, J.-F. Bu, C.-J. Lin, G.-L. Song, Recent progress in corrosion protection of magnesium alloys by organic coatings, Progress in Organic Coatings 73 (2–3) (2012) 129–141.

[27] T.F. da Conceicao, N. Scharnagl, W. Dietzel, K.U. Kainer, Corrosion protection of magnesium AZ31 alloy using poly(ether imide) [PEI] coatings prepared by the dip coating method: Influence of solvent and substrate pre-treatment, Corrosion Science 53 (1) (2011) 338–346.

[28] U.C. Nwaogu, C. Blawert, N. Scharnagl, W. Dietzel, K.U. Kainer, Effects of organic acid pickling on the corrosion resistance of magnesium alloy AZ31 sheet, Corrosion Science 52 (6) (2010) 2143–2154.

[29] H.H. Elsentriecy, K. Azumi, H. Konno, Effect of surface pretreatment by acid pickling on the density of stannate conversion coatings formed on AZ91 D magnesium alloy, Surface and Coatings Technology 202 (3) (2007) 532–537.

[30] R. Supplit, T. Koch, U. Schubert, Evaluation of the anti-corrosive effect of acid pickling and sol–gel coating on magnesium AZ31 alloy, Corrosion Science 49 (7) (2007) 3015–3023.

[31] Q. Qu, J. Ma, L. Wang, L. Li, W. Bai, Z. Ding, Corrosion behaviour of AZ31B magnesium alloy in NaCl solutions saturated with CO_2, Corrosion Science 53 (4) (2011) 1186–1193.

[32] F. Zucchi, V. Grassi, A. Frignani, C. Monticelli, G. Trabanelli, Influence of a silane treatment on the corrosion resistance of a WE43 magnesium alloy, Surface and Coatings Technology 200 (12–13) (2006) 4136–4143.

[33] C. Trepanier, M. Tabrizian, L.H. Yahia, L. Bilodeau, D.L. Piron, Effect of modification of oxide layer on NiTi stent corrosion resistance, Journal of Biomedical Materials Research 43 (4) (1998) 433–440.

[34] N. Huang, P. Yang, Y.X. Leng, J.Y. Chen, H. Sun, J. Wang, G.J. Wang, P.D. Ding, T.F. Xi, Y. Leng, Hemocompatibility of titanium oxide films, Biomaterials 24 (13) (2003) 2177–2187.

[35] Y. Xin, Corrosion behavior of biomedical AZ91 magnesium alloy in simulated body fluids, Journal of Materials Research 22 (7) (2007) 2004–2011.

[36] A. Abdal-hay, F.A. Sheikh, J.K. Lim, Air jet spinning of hydroxyapatite/poly (lactic acid) hybrid nanocomposite membrane mats for bone tissue engineering, Colloids and Surfaces B: Biointerfaces 102 (0) (2013) 635–643.

[37] A. Abdal-hay, L.D. Tijing, J.K. Lim, Characterization of the surface biocompatibility of an electrospun nylon 6/CaP nanofiber scaffold using osteoblasts, Chemical Engineering Journal 215–216 (0) (2013) 57–64.

[38] G.S. Lodha, V.K. Raghuvanshi, M.H. Modi, P. Tripathi, A. Verma, R. V. Nandedkar, X-ray multilayer optics: growth and characterization, Vacuum 60 (4) (2001) 385–388.

[39] K. Cai, M. Müller, J. Bossert, A. Rechtenbach, K.D. Jandt, Surface structure and composition of flat titanium thin films as a function of film thickness and evaporation rate, Applied Surface Science 250 (1–4) (2005) 252–267.

[40] S. Chen, S. Guan, S. Hou, L. Wang, S. Zhu, J. Wang, W. Li, Characterization and corrosion properties of Ti-O/HA composite coatings on Mg–Zn alloy, Surface and Interface Analysis 43 (13) (2011) 1575–1580.
[41] J. Choueka, J.L. Charvet, K.J. Koval, H. Alexander, K.S. James, K. A. Hooper, J. Kohn, Canine bone response to tyrosine-derived polycarbonates and poly(L-lactic acid), Journal of Biomedical Materials Research 31 (1) (1996) 35–41.
[42] A. Abdal-Hay, M. Dewidar, J.K. Lim, Biocorrosion behavior and cell viability of adhesive polymer coated magnesium based alloys for medical implants, Applied Surface Science 261 (2012) 536–546.
[43] N. Scharnagl, C. Blawert, W. Dietzel, Corrosion protection of magnesium alloy AZ31 by coating with poly(ether imides) (PEI), Surface and Coatings Technology 203 (10–11) (2009) 1423–1428.
[44] P.A. Sørensen, S. Kiil, K. Dam-Johansen, C.E. Weinell, Anticorrosive coatings: a review, Journal of Coatings Technology and Research 6 (2) (2009) 135–176.
[45] A. Abdal-hay, N.A.M. Barakat, J.K. Lim, Influence of electrospinning and dip-coating techniques on the degradation and cytocompatibility of Mg-based alloy, Colloids and Surfaces A: Physicochemical and Engineering Aspects 420 (0) (2013) 37–45.
[46] A. Abdal-hay, T. Amna, J.K. Lim, Biocorrosion and osteoconductivity of PCL/nHAp composite porous film-based coating of magnesium alloy, Solid State Sciences 18 (0) (2013) 131–140.
[47] F. Witte, H. Ulrich, M. Rudert, E. Willbold, Biodegradable magnesium scaffolds: Part 1: appropriate inflammatory response, Journal of Biomedical Materials Research A 81 (3) (2007) 748–756.
[48] X. Zhang, G. Yuan, L. Mao, J. Niu, P. Fu, W. Ding, Effects of extrusion and heat treatment on the mechanical properties and biocorrosion behaviors of a Mg–Nd–Zn–Zr alloy, Journal of the Mechanical Behavior of Biomedical Materials 7 (2012) 77–86.
[49] C. Lorenz, J.G. Brunner, P. Kollmannsberger, L. Jaafar, B. Fabry, S. Virtanen, Effect of surface pre-treatments on biocompatibility of magnesium, Acta Biomaterialia 5 (7) (2009) 2783–2789.